Available online at www.sciencedirect.com
SCIENCE DIRECT®
ELSEVIER Applied Mathematics and Computation 167 (2005) 383–418
APPLIED MATHEMATICS AND COMPUTATION
www.elsevier.com/locate/amc

Option valuation by using discrete singular convolution

Shan Zhao [a,*], G.W. Wei [a,b]

[a] *Department of Mathematics, Michigan State University, East Lansing, MI 48824, USA*
[b] *Department of Electrical and Computer Engineering, Michigan State University, East Lansing, MI 48824, USA*

Abstract

This paper explores the utility of a discrete singular convolution (DSC) algorithm for solving the Black–Scholes equation. Both European and American style options, which include all nontrivial plain option pricing problems, are considered to test the accuracy and to examine the efficiency of the present algorithm. Adaptive meshes are constructed to enhance the performance of the DSC algorithm. All the present results are validated either by the analytical solution or by the standard binomial tree method. Extensive comparisons are carried out with two standard finite difference schemes and two binomial models of high speed convergence. Numerical experiments reveal that the present approach is accurate, efficient and reliable for financial derivative valuations.

Keywords: Option pricing; Discrete singular convolution; Adaptive mesh; American option valuation; Optimal exercise boundary

* Corresponding author.
E-mail addresses: szhao@math.msu.edu (S. Zhao), wei@math.msu.edu (G.W. Wei).

0096-3003/$ - see front matter
doi:10.1016/j.amc.2004.07.010

Nomenclature

B	frequency bound
c	DSC parameter, β/Δ
D	dividend amount
D_1, D_2, D_3	dividend amounts in multiple discrete dividends paying case
f	L^2 function
F	generic function
F_α	an approximation to F
$\mathbf{G}_{\mathrm{DSC}}$	DSC approximation matrix
H	number of the underlying asset
K	distribution
K_α	distribution approximation sequence
l	approximation parameter of distribution sequence (integer)
$\mathscr{L}$	linear differential operator
L_∞	maximum absolute error measure
L_2	root mean squared error measure
M	discretization parameter of Dirichlet type kernels
N	total grid number
N_{bt}	total number of time steps in the binomial tree method
$N(\cdot)$	standard normal distribution function
$N_2(\cdot,\cdot;\cdot)$	standard bivariate normal distribution function
q	continuous dividend payout rate
r	riskless interest rate
$\mathbf{r}_1$, $\mathbf{r}_2$, $\mathbf{r}_3$, $\boldsymbol{r}_4$	temporary variables used in the Runge–Kutta scheme
$R_\beta(\cdot)$	regularizer
S	stock price, asset price
S_T	stock price at date T
$\tilde{S}$	risky component of an asset price
$[\tilde{S}^*]$	asset node on the coarse grid, which has the smallest distance departed from the critical price $\tilde{S}^*$ among all coarse grid nodes.
t	time
T	time of expiration
v	option value
v_m	the spatial discretization of v with respect to the x-coordinate
$\bar{v}$	option value directly calculated from the last time step
$\mathbf{v}$	$(v_1, v_2, \ldots, v_m, \ldots, v_N)$
W	half bandwidth
x_k	discrete sampling points around the point x
X	strike price
Z	random variable following the standard Wiener process

Greek

α	approximation parameter of distribution sequence
β	width of the Gaussian envelope
δ	delta distribution
$\delta_{\alpha,\beta;k}$, $\delta_{\frac{\pi}{\Delta},\beta;k}$	convolution kernels
Δ	grid spacing, incremental value
$\bar{\Delta}$	$(3/2)\Delta$
η	element of the space of test functions
μ	expected rate of return
∂	partial
Π	portfolio
ρ	correlation coefficients
σ	volatility
τ	time to expiration
τ_d	single ex-dividend date
τ_1, τ_2, τ_3	ex-dividend dates in a multiple discrete dividends paying case
τ_1^*, τ_2^*, τ_3^*	critical dates of the optimal exercise boundary in a multiple discrete dividends paying case
θ	desired significant figure index

subscripts

i, j, k	iteration labels
min, max	the left and right boundaries of the asset price coordinate
s, e	the starting and ending dates of a finer grid

superscripts

d	index of the finer grid used in the valuation of American calls on discrete dividend paying assets
l	the level index of a finer grid
(n)	nth derivative
$+$, $-$	instants immediately after and before certain date
$*$	critical asset price
$\wedge$	numerical estimated value

1. Introduction

Option pricing is often modeled by stochastic processes, from which partial differential equations (PDEs), such as the Black–Scholes equation, can be derived under appropriate assumptions [5,31]. It is well known that many important derivatives lack a closed-form analytical solution and their estimation has

to be performed by numerical procedures. For this purpose, three major numerical approaches have been developed in the finance literature: binomial tree model [15], finite difference (FD) method [7,8,34], and Monte Carlo simulation [6]. Apart from numerical methods, a number of analytical approximation methods have been also suggested in the literature, especially for pricing American options, such as the quadratic approximation approach [30,4], compound option approximation [18,11], the method of interpolation between bounds [24,9], and the analytic method of lines [12]. Generally speaking, both the binomial tree method and the Monte Carlo simulation approximate the underlying stochastic processes directly, while the FD scheme and analytic approximation are used to solve the Black–Scholes equation with appropriate boundary conditions that characterize various option pricing problems. Some detailed review and/or comparison of the alternative option valuation techniques are available in [19,9].

Commonly used numerical methods, such as the FD scheme and the binomial tree method, are quite simple, flexible, and convergent (as was proved in [22,1]) for financial derivatives. However, the speed of convergence of these methods is usually very slow. Recently, two explicit FD schemes, a fully explicit FD scheme [7,34] and a widely used mixed FD scheme [8,21], are carefully examined by Buetow and Sochacki [10] for their use in pricing derivative securities. They found that for European option valuation, the relative error between mixed and explicit FD schemes becomes financially significant. In this valuation, the approximation errors of two FD schemes could be actually *much larger* than (sometimes up to 39 times) the relative error, and such mispricing may become worse in some complicated cases. Therefore, under certain requirements, it will be very expensive to achieve acceptable accuracy in option valuations by using lower-order approximation schemes.

Much effort has been made to improve the binomial model. One aspect concerns the speed of convergence of lattice approach [23,38]. Leisen and Reimer [28] measured the speed of convergence by using the concept of order of convergence, and showed that the lattice approaches given in [23] and in [38] have the same order of convergence (order one), as the original binomial model [15] for the valuation of European options. Recently, two extended lattice approaches have been constructed by Leisen and Reimer [28] and Leisen [26] which can numerically achieve second order of convergence in European option valuation, and first order in American put valuation with small initial error. More recently, by treating the difference between two trading dates as being random, a delicately designed random-time binomial model was constructed [27], which can speed the convergence up to second order in American put valuation. The other aspect seeks to improve the accuracy of the binomial model. Figlewski and Gao [16] introduced an adaptive mesh model to the conventional lattice approaches. Their idea is to utilize a higher-resolution lattice in the critical region where discretization evokes severe approximation errors,

while keeping the use of a coarser gird for the rest of the mesh. The accuracy can be improved significantly with a relatively small additional computational effort.

The utility of adaptive mesh can be justified from both financial and numerical considerations. For a plain call or put, very rapid changes in the option price occur around the strike price at expiration. Gamma value of an at-the-money option will increase without limit as the time to maturity tends to zero so that the value of a option holder's position shortly before expiration is highly sensitive to jumps in the stock price. Numerically, it is the rapid changes in this critical region that introduce the most serious discretization error and the final maximum numerical error always occurs around the at-the-money option. In practice, such an option is of great interest to both academicians and practitioners compared with other deep in-the-money and out-of-the-money options. Thus, the problem of accurate resolution of the high gradient region is important not only from the consideration of truncation error but also from the viewpoint of finance.

Much effort has also been made to improve the FD schemes. Most of them are mainly focus on improving the accuracy of the FD schemes. For example, by using a coordinate transformation which yields high resolution nodes around a strike price, Clarke and Parrott [13] found that the accuracy and performance of their implicit FD scheme could be improved considerably. Obviously, their technique is essentially similar to the adaptive mesh method used for the binomial model. The other interesting way to improve the FD schemes is utilizing higher order numerical PDE schemes. For the lower-order FD scheme used in the finance literature, the error of the scheme may be substantial, limiting the performance of adaptive mesh techniques. However, higher-order FD schemes are usually cumbersome to implement in association with special boundary conditions, which often occur in option pricing problems.

Recently, the discrete singular convolution (DSC) algorithm [42] has been developed as a wavelet-collocation approach [43] for solving various challenging computational problems in fluid dynamics simulation [40], structural analysis [46,47], computational electromagnetics [2,37,3], and shock capturing [45,48]. The mathematical foundation of the algorithm is the theory of distributions and the theory of wavelets [44]. It has been shown that in the framework of the DSC algorithm, the wavelet collocation is equivalent to a wavelet Galerkin [43]. By appropriately selecting parameters of a DSC kernel, the DSC approach exhibits spectral accuracy for integration [32,2,3] and shows great flexibility in handling complex geometries and boundary conditions [40,47,37,48].

The objective of the present work is twofold. First, we explore the use of the DSC algorithm as an alternative approach for solving the Black–Scholes equation directly. The present DSC approach provides a simple, systematic algorithm for the generation of FD schemes of an arbitrary order. Second, we

study the efficiency enhancement of both the conventional FD scheme and the DSC approach under adaptive meshes.

This paper is organized as follows. Section 2 is devoted to a brief review of the option pricing model and the DSC algorithm. The implementation of the DSC algorithm for the option pricing model is discussed. Section 3 presents the applications of the DSC approach to the solution of the Black–Scholes equation. We use both European and American options to illustrate the present approach. The benchmark problem, European option pricing, is used since it enable us to assess the accuracy of the numerical approximation against the exact Black–Scholes value. The American options which are the most popularly traded options on exchanges are also treated in this study. Different dividend paying conditions, which cover all nontrivial plain options, are tested. Two high accuracy lattice approaches and two standard FD methods are implemented for a comparison. Both the analytical solution and the conventional binomial model are invoked for a quantitative validation of the present approach. Conclusions are given in Section 4. Some algebraic details are presented in Appendices.

2. Theory and algorithms

In this section, we first describe a mathematical model of option pricing. The DSC algorithm is introduced for solving the Black–Scholes equation. Some computational aspects, including the finite difference schemes, are discussed.

2.1. The Black–Scholes equation

The starting point of the mathematical theory of option pricing is the random walk assumption for the asset price, i.e. the evolution of the asset price S at time t follows the geometric Brownian motion

$$\frac{\mathrm{d}S}{S} = \mu\,\mathrm{d}t + \sigma\,\mathrm{d}Z, \tag{1}$$

where μ is the expected rate of return and σ is the volatility, and $\mathrm{d}Z$ is the standard Wiener process with a zero mean and variance $\mathrm{d}t$. By adopting the common hedging procedure, a portfolio Π which consists of one option v and a number $-H$ of the underlying asset is formed

$$\Pi = v - HS. \tag{2}$$

By setting $H = \partial v/\partial S$, it can be shown that the portfolio Π becomes a riskless hedge. In an efficient market with no riskless arbitrage opportunity, any portfolio with a zero market risk must have an expected rate of return which equals the riskless interest rate r. Therefore we have $\mathrm{d}\Pi = r\Pi\mathrm{d}t$. In a complete form, we arrive at the Black–Scholes equation [5]

$$\frac{\partial v}{\partial t}+\frac{\sigma^2}{2}S^2\frac{\partial^2 v}{\partial S^2}+rS\frac{\partial v}{\partial S}-rv=0,\quad 0<S<\infty,\ t>0. \tag{3}$$

The general form of the Black–Scholes equation which is used in the present numerical study is given by:

$$\frac{\partial v}{\partial \tau}=\frac{\sigma^2}{2}S^2\frac{\partial^2 v}{\partial S^2}+(r-q)S\frac{\partial v}{\partial S}-rv,\quad 0<S<\infty,\ \tau>0, \tag{4}$$

where q is the continuous dividend payout rate, τ is the time to expiration ($\tau = T - t$), and T is the time of expiration. Eq. (4) along with various initial and boundary conditions (expiration, exercise, and payout conditions) is used to characterize different options.

2.2. Discrete singular convolution

The underlying mathematical structure of the DSC approach is the theory of distributions. Singular convolutions are essential to many science and engineering problems, such as electromagnetics, Hilbert transform, Abel transform and Radon transform. The DSC algorithm is a general approach for numerically solving singular convolution problems. By an appropriate construction of singular convolution kernels, the DSC can be an extremely efficient, accurate and reliable algorithm for practical applications [42].

The simplest way to introduce the theory of *singular convolution* is to work in the context of distributions. The latter has important ramifications in mathematical analysis [44]. Let K be a distribution and η be an element of the space of test functions. A singular convolution is defined as:

$$F(t)=\int_{-\infty}^{\infty}K(t-x)\eta(x)\,\mathrm{d}x. \tag{5}$$

Here $K(t - x)$ is a singular kernel. Depending on the form of the kernel K, the singular convolution is the central issue for a wide range of science and engineering problems. For example, singular kernels of the Hilbert type have a general form of

$$K(x)=\frac{1}{x^n}\quad (n>0). \tag{6}$$

Here, kernels $K(x) = 1/x^{\alpha}$ $(0 < \alpha < 1)$ define the *Abel transform* which is closely connected with a generalization of the tautochrone problem. Kernel $K(x) = 1/x$ is commonly encountered in electrodynamics, theory of linear response, signal processing, theory of analytic functions and the Hilbert transform; $K(x) = 1/x^2$ is the kernel popularly used in tomography. The other interesting example is the singular kernels of the delta type

$$K(x)=\delta^{(n)}(x)\quad (n=0,1,2,\ldots). \tag{7}$$

Here, kernel $K(x) = \delta(x)$ is of particular importance for the interpolation of surfaces and curves (including atomic, molecular and biological potential energy surfaces, and for numerous image processing and pattern recognition problems) and $K(x) = \delta^{(n)}(x)$, ($n = 1,2,\ldots$) are essential for obtaining weak solutions of partial differential equations. However, since these kernels are singular, they cannot be directly digitized in numerical computation. Hence, the singular convolution, (5), is of little numerical merit. To avoid the difficulty of using singular expressions directly in computation, sequences of approximations $\{K_\alpha\}$ of the distribution K can be constructed:

$$\lim_{\alpha\to\alpha_0} K_\alpha(x) \to K(x), \tag{8}$$

where α_0 is a generalized limit. Obviously, in the case of $K(x) = \delta(x)$, the sequence, $K_\alpha(x)$, is a delta sequence. It is noted that at the limit one retains the delta distribution, which is a real constant in the frequency space and is the so-called *all pass filter*. Computationally, the delta distribution is a *universal reproducing kernel* which can be used as a starting point for the construction of either band-limited reproducing kernels or approximate reproducing kernels. Further more, with a sufficiently smooth approximation, it is useful to consider a *discrete singular convolution* (DSC)

$$F_\alpha(t) = \sum_k K_\alpha(t - x_k) f(x_k), \tag{9}$$

where $F_\alpha(t)$ is an approximation to $F(t)$ and $\{x_k\}$ is an appropriate set of discrete points on which the discrete convolution (9) is well-defined. It is this discrete expression that makes a computational realization possible. Note that the original test function $\eta(x)$ has been replaced by $f(x)$. The mathematical property or requirement of $f(x)$ is determined by the approximate kernel K_α. In general, the convolution is required to be Lebesgue integrable.

It is helpful to illustrate the algorithm by examples. A simple example is Shannon's kernel [36], $(\sin \alpha x)/\pi x$, which is also known as Sinc function [29]. Shannon's kernels are a delta sequence and thus provide an approximation to the delta distribution or so-called Dirac delta function δ

$$\lim_{\alpha\to\infty} \left\langle \frac{\sin \alpha x}{\pi x}, \eta(x) \right\rangle = \eta(0), \tag{10}$$

where $\langle \cdot, \cdot \rangle$ denotes the standard inner product. As another important example, Lagrange kernel is of great interest, since the corresponding DSC approach provides a simple, systematic algorithm for the generation of FD schemes of an arbitrary order [43]:

$$\prod_{i=-\infty, i\neq k}^{\infty} \frac{x - x_i}{x_k - x_i}, \quad k \in \mathbb{Z}. \tag{11}$$

Other important examples include the Dirichlet kernel

$$\frac{\sin\left[\left(l+\frac{1}{2}\right)x\right]}{2\pi\sin\left[\frac{1}{2}x\right]}, \quad l=0,1,2,\ldots, \tag{12}$$

the modified Dirichlet kernel

$$\frac{\sin\left[\left(l+\frac{1}{2}\right)x\right]}{2\pi\tan\left[\frac{1}{2}x\right]}, \quad l=0,1,2,\ldots, \tag{13}$$

and the de la Vallée Poussin kernel

$$\frac{1}{\pi}\frac{\cos[\alpha x]-\cos[2\alpha x]}{x^2}. \tag{14}$$

For sequences of both the delta type and the Hilbert type, an interpolating (or quasi-interpolating) algorithm sampling at Nyquist frequency, $\alpha=\pi/\Delta$, has great advantage over a non-interpolating discretization. Therefore, Shannon's kernel is discretized as

$$\frac{\sin\alpha x}{\pi x}\to\frac{\sin\frac{\pi}{\Delta}(x-x_k)}{\frac{\pi}{\Delta}(x-x_k)}. \tag{15}$$

In fact, the interpolative (or quasi-interpolative) nature not only guarantees the highest accuracy on the set of grid points, but provides the highest possible computational efficiency of a grid as well. This is because the Nyquist interval given by $[-\pi/\Delta,\pi/\Delta]$ is the largest possible sampling interval that is free of alias whenever the L^2 function $f(x)$ under study satisfies the *Nyquist condition*:

$$\operatorname{supp}\hat{f}(k)\subset\left\{-\frac{\pi}{\Delta},\frac{\pi}{\Delta}\right\}. \tag{16}$$

This fact can be formally addressed by Shannon's sampling theorem

$$f(x)=\sum_{k=-\infty}^{\infty}f(x_k)\frac{\sin\frac{\pi}{\Delta}(x-x_k)}{\frac{\pi}{\Delta}(x-x_k)}. \tag{17}$$

The significance of Shannon's sampling theorem is that by a discrete, but infinite set of sampling data, $\{f(x_k)\}$, one can actually recover a band-limited L^2 function on a real line. Such band-limited L^2 functions are known as elements of the Paley–Wiener reproducing kernel Hilbert space. The discrete Shannon's kernel, $\{\sin\frac{\pi}{\Delta}(x-x_k)/\frac{\pi}{\Delta}(x-x_k)\}_{k\in\mathbb{Z}}$, are a complete set of sampling basis. Shannon's sampling theorem has great impact on information theory, signal and image processing because the Fourier transform of Shannon's kernel is an ideal low-pass filter for signals band-limited to $[-\pi/\Delta,\pi/\Delta]$.

The uniform, Nyquist rate, interpolating discretization is also used for the Dirichlet kernel [42]:

$$\frac{\sin\left[\left(l+\frac{1}{2}\right)x\right]}{2\pi\sin\left[\frac{1}{2}x\right]}\to\frac{\sin\left[\frac{\pi}{\Delta}(x-x_k)\right]}{(2M+1)\sin\left[\frac{\pi}{\Delta}\frac{x-x_k}{2M+1}\right]}. \tag{18}$$

In comparison to Shannon's kernel, the Dirichlet kernel has one more parameter M which can be optimized to achieve better results in computations. Usually, we set a sufficiently large M for various numerical applications. Obviously, the Dirichlet kernel converts to Shannon's kernel at the limit of $M \to \infty$. This uniform interpolating discretization will also be used for discretizing the modified Dirichlet kernels

$$\frac{\sin\left[\left(l+\frac{1}{2}\right)x\right]}{2\pi\tan\left[\frac{1}{2}x\right]} \to \frac{\sin\left[\frac{\pi}{\Delta}(x-x_k)\right]}{(2M+1)\tan\left[\frac{\pi}{\Delta}\frac{x-x_k}{2M+1}\right]} \tag{19}$$

and for the de la Vallée Poussin kernel

$$\frac{1}{\pi}\frac{\cos[\alpha x]-\cos[2\alpha x]}{x^2} \to \frac{2}{3}\frac{\cos\left[\frac{\pi}{\Delta}(x-x_k)\right]-\cos\left[\frac{2\pi}{\Delta}(x-x_k)\right]}{\left[\frac{\pi}{\Delta}(x-x_k)\right]^2}, \tag{20}$$

where $\overline{\Delta} = (3/2)\Delta$. Since π/Δ is proportional to the highest frequency which can be reached in the Fourier representation, the Δ should be very small for a given problem involving highly oscillatory functions or very high frequency components. In other words, a very high resolution mesh is expected for some critical region where very rapid changes in the solution occur. It is also noted that, if the discrete points $\{x_i\}_{i=-\infty}^{\infty}$ in the Lagrange kernel are uniformly distributed grid points, the Lagrange kernel (11) is already in its form of a uniform and interpolating discretization.

It is noted that the sequence of approximation can be improved by a function $R_\beta(x)$ [41] that has the property

$$\lim_{\beta\to\infty} R_\beta(x) = 1. \tag{21}$$

$R_\beta(x)$ is called a regularizer when (21) is satisfied. The regularizer is designed to increase the regularity of convolution kernels. For the delta sequence, it follows from Eq. (8) that

$$\int \lim_{\alpha\to\alpha_0} K_\alpha(x) R_\beta(x)\,\mathrm{d}x = R_\beta(0) = 1, \tag{22}$$

where $R_\beta(0) = 1$ is the special requirement for a *delta regularizer*. A typical delta regularizer used in this work and elsewhere [41] is $\exp(-x^2/2\beta^2)$. Consequently, Shannon's kernel is regularized as

$$\frac{\sin\frac{\pi}{\Delta}(x-x_k)}{\frac{\pi}{\Delta}(x-x_k)} \to \frac{\sin\frac{\pi}{\Delta}(x-x_k)}{\frac{\pi}{\Delta}(x-x_k)}\mathrm{e}^{-((x-x_k)^2/2\beta^2)}. \tag{23}$$

Since $\exp(-x^2/2\beta^2)$ is a Schwartz class function, it makes the regularized kernel applicable to tempered distributions. Numerically, the regularized expression performs much better than Shannon's kernel for solving PDEs [41].

Usually, a symmetrically (or antisymmetrically) truncated DSC kernel is used to approximate the nth order derivative of a function $f(x)$ as follows

$$f^{(n)}(x) \approx \sum_{k=-W}^{W} \delta^{(n)}_{\alpha,\beta;k}(x) f(x_k), \quad n = 0, 1, 2, \ldots, \tag{24}$$

where $2W + 1$ is the computational bandwidth, or effective kernel support, which is usually smaller than the whole computational domain. Here $\delta^{(n)}_{\alpha,\beta;k}(x)$ is the nth derivative of $\delta_{\alpha,\beta;k}(x)$, which is a collective symbol for any of the right-hand side of Eqs. (15) (or (23)), (18)–(20) and the finite Lagrange kernel

$$L_k(x) = \prod_{i=-W, i\neq k}^{W} \frac{x - x_i}{x_k - x_i}. \tag{25}$$

It can be shown that the finite Lagrange kernel is also a delta kernel as the $\max_{\forall i}|x_{i+1} - x_i| \to 0$ for a sufficiently large W [44].

A mathematical estimation of approximation errors for the regularized Shannon's kernel has recently been provided in [32]. In particular, it is proved that the truncation error of the DSC algorithm by using the regularized Shannon's kernel decays exponentially with respect to the increase in sampling points. In other words, the DSC algorithm can also achieve spectral accuracy of global methods. This theoretical estimation is in excellent agreement with previous numerical tests [41,43,2,48,3].

2.3. Numerical implementation

In this subsection, we describe the implementation of the DSC algorithm for the spatial and temporal discretizations of the Black–Scholes equation. Two finite-difference based schemes are also presented for a comparison.

Without the loss of generality, we consider a generic linear PDE of the form

$$v_t + \mathscr{L}v + F(v) = 0, \tag{26}$$

where $F(v)$ is a source term and $\mathscr{L}$ is a linear differential operator. In the DSC approach, it is convenient to discretize an operator on a grid of the coordinate representation and to use the collocation approach for solving a PDE [43]. Therefore, the source term can be discretized by

$$[F(v)]_{x=x_m} = F(v_m), \tag{27}$$

where the (integer) subscript v_m denotes the spatial discretization of v with respect to the x-coordinate. In terms of the DSC approximation Eq. (24), the differential operator can be represented by the convolution

$$[\mathscr{L}v]_{x=x_m} = \sum_n \left[d_n(x) \frac{\partial^n v}{\partial x^n} \right]_{x=x_m} = \sum_n d_n(x_m) \sum_{k=m-W}^{m+W} \delta^{(n)}_{\alpha,\beta;k}(x_m) v_k, \tag{28}$$

where $d_n(x)$ is a coefficient and $\delta^{(n)}_{\alpha,\beta;k}(x_m)$ is *analytically* given by

$$\delta^{(n)}_{\alpha,\beta;k}(x_m) = \left[\left(\frac{\mathrm{d}}{\mathrm{d}x}\right)^n \delta_{\alpha,\beta;k}(x)\right]_{x=x_m}. \tag{29}$$

Some detailed expressions of these derivatives are given in Appendix A.

Therefore, a DSC semi-discrete form of the genetic equation can be expressed as

$$\frac{\mathrm{d}v_m}{\mathrm{d}t} = -\sum_n d_n(x_m) \sum_{k=m-W}^{m+W} \delta^{(n)}_{\alpha,\beta;k}(x_m) v_k - F(v_m). \tag{30}$$

To take into account for the temporal discretization, Eq. (30) can be rewritten in its vector form

$$\frac{\mathrm{d}\mathbf{v}}{\mathrm{d}t} = \mathbf{G}_{\mathrm{DSC}}(\mathbf{v}, t), \tag{31}$$

where $\mathbf{v} = (v_1, v_2, \ldots, v_m, \ldots, v_N)$ and $\boldsymbol{G}_{\mathrm{DSC}}(\boldsymbol{v},t)$ represents the DSC approximation in the right-hand side of Eq. (30).

The commonly used time stepping schemes, either explicit or implicit, can be easily used along with the DSC algorithm. In the present study, two explicit time discretization methods, the explicit Euler scheme and the classical fourth-order Runge–Kutta method, are employed. For the explicit Euler scheme, $\boldsymbol{v}$ can be evaluated as

$$\mathbf{v}^{j+1} = \mathbf{v}^j + \Delta t \mathbf{G}_{\mathrm{DSC}}(\mathbf{v}^j, t_j) \tag{32}$$

at each time step, while for the Runge–Kutta method

$$\mathbf{v}^{j+1} = \mathbf{v}^j + \tfrac{1}{6}(\mathbf{r}_1 + 2\mathbf{r}_2 + 2\mathbf{r}_3 + \mathbf{r}_4), \tag{33}$$

in which

$$\mathbf{r}_1 = \Delta t \mathbf{G}_{\mathrm{DSC}}(\mathbf{v}^j, t_j), \quad \mathbf{r}_2 = \Delta t \mathbf{G}_{\mathrm{DSC}}\left(\mathbf{v}^j + \tfrac{1}{2}\mathbf{r}_1, t_j + \tfrac{1}{2}\Delta t\right), \tag{34}$$

$$\mathbf{r}_3 = \Delta t \mathbf{G}_{\mathrm{DSC}}(\mathbf{v}^j + \tfrac{1}{2}\mathbf{r}_2, t_j + \tfrac{1}{2}\Delta t), \quad \mathbf{r}_4 = \Delta t \mathbf{G}_{\mathrm{DSC}}(\mathbf{v}^j + \mathbf{r}_3, t_j + \Delta t). \tag{35}$$

In the present study, we focus our attention on two DSC kernels, although various other delta sequence kernels can be similarly employed [43]. The first kernel considered is a regularized Shannon's kernel (RSK), Eq. (23), which has been extensively used in the previous DSC calculations. When we set $W = 1$, the present DSC weights, $\delta^{(n)}_{\alpha,\beta;k}(x)$, can always be made exactly the same as those of the second-order central difference scheme (i.e. $\frac{1}{2\Delta}$, 0, $-\frac{1}{2\Delta}$ for the first-order derivative and $\frac{1}{\Delta^2}$, $-\frac{2}{\Delta^2}$, $\frac{1}{\Delta^2}$ for the second-order derivative) of the standard FD method by choosing the parameter β appropriately. Another DSC kernel studied is the Lagrange kernel (LK), Eq. (25). The regularity of the LK can be increased by using a regularizer as in (23) and the corresponding DSC approximation can be optimized in a practical application by varying β

[43]. However, to achieve a comparison between the DSC approach and the traditional FD scheme, the ordinary LK is used. The half bandwidth W is chosen as $W = 32$ for both LK and RSK in the present study, and β is set to $\beta = 3.5\Delta$ in the RSK.

For a comparison, two conventional FD schemes, the explicit FD (EFD) and Crank–Nicolson (CN) schemes, are also used to numerically evaluate the European and American options. The EFD form of Eq. (4) is of the explicit Euler scheme for the time discretization and the central difference scheme for the spatial discretization [7,34,10]

$$\frac{v_i^{j+1} - v_i^j}{\Delta\tau} = \frac{\sigma^2}{2} S_i^2 \frac{v_{i+1}^j - 2v_i^j + v_{i-1}^j}{(\Delta S)^2} + (r-q) S_i \frac{v_{i+1}^j - v_{i-1}^j}{2\Delta S} - r v_i^j, \tag{36}$$

where i and j are indices of stock price node and time to expiration instant, respectively. The CN discretization form of Eq. (4) is [14]

$$\begin{aligned} \frac{v_i^{j+1} - v_i^j}{\Delta\tau} = {} & \frac{\sigma^2}{4} S_i^2 \left(\frac{v_{i+1}^{j+1} - 2v_i^{j+1} + v_{i-1}^{j+1}}{(\Delta S)^2} + \frac{v_{i+1}^j - 2v_i^j + v_{i-1}^j}{(\Delta S)^2} \right) \\ & + \frac{(r-q)}{4} S_i \left(\frac{v_{i+1}^{j+1} - v_{i-1}^{j+1}}{\Delta S} + \frac{v_{i+1}^j - v_{i-1}^j}{\Delta S} \right) - r \frac{v_i^{j+1} + v_i^j}{2}. \end{aligned} \tag{37}$$

Two extended lattice approaches are also studied for non-dividend paying cases of European and American option valuation problems in the present paper. A comparison between traditional binomial models and PDE methods has been made by Geske and Shastri [19]. In the present study, we are particularly interested in a comparison between the high order convergence lattice approaches and the DSC scheme. One lattice approach is the PP2 method of Leisen and Reimer [28], and is denoted as PP method in the present study. The other one is the smooth version (SMO) of the binomial model of Cox et al. [15], which was suggested by Leisen [26]. The extrapolation technique is also used as in the original papers. These two lattice approaches can numerically exhibit order of convergence two for European option valuation, and much smaller initial errors for American option valuation. The random-time binomial model [27] will not be considered in the present study, since the time increment is fixed for other methods.

3. Experimental studies

To illustrate the utility of the DSC algorithm and to test its accuracy for option valuation, both European and American option valuation problems are investigated in the present study. The cases under study essentially cover all plain option pricing problems. To comprehensively examine the performance of the DSC algorithm in solving Black–Scholes equation, the original model

with variable coefficients is studied in the present paper, which is more difficult to solve numerically than the one with constant coefficients [19].

For all types of option pricing problems, three maturity times, $T = 1$, 4, and 7 months, are tested. Other model parameters except dividend payment conditions are fixed as: $r = 5.0\%$, $\sigma = 0.3$ and strike price $X = 45$. The greatest error and the overall accuracy of the approximations are measured, respectively, by using the maximum absolute error measure,

$$L_\infty = \max_{i=1,\ldots,N} |\hat{v}_i - v_i|, \tag{38}$$

and the root mean squared error measure,

$$L_2 = \sqrt{\frac{1}{N}\sum_{i=1}^{N} (\hat{v}_i - v_i)^2}, \tag{39}$$

where N is the total grid number, v_i is the exact Black–Scholes value or benchmark value, and $\hat{v}_i$ is the numerically estimated option price. All numerical experiments are conducted on a digital Alpha 600 MHz personal workstation. To estimate the computational efficiency, the execution time (ET) of every tested case is calculated as the approximate CPU time for single option with the expiration date $T = 7$ months and measured in seconds.

To discretize Eq. (4), a uniform mesh is constructed on the stock price-time hyperplane, from $S = S_{\min} = 0$ to $S = S_{\max}$ with a spacing ΔS, and from $\tau = 0$ to $\tau = T$ with a time increment $\Delta\tau$. In all cases, unless otherwise specified, the uniform stock price-time mesh employed in the present study is constructed as follows. For European option valuation: $\Delta S = 0.5$, $S_{\max} = 200$, and $\Delta\tau = 5.0 \times 10^{-4}$ (or denoted as $\Delta\ \tau = 5.0(-4)$) month; For American option valuation: $\Delta S = 0.5$, $S_{\max} = 140$, and $\Delta\tau = 5.0(-4)$ month.

3.1. European option

The benchmark problem, European option valuation, is of great interest to academicians in the finance literature. It is often utilized to test the accuracy of a given numerical scheme [19,16,10]. Both call and put options are studied for the problem of European option pricing.

3.1.1. European call option

Three types of valuation problems for European call options are treated: European calls on non-dividend paying assets (ECND), European calls on continuous dividend paying assets (ECCD), and European calls on discrete dividend paying assets (ECDD). The value of a European call option can be determined by solving Eq. (4) subject to the initial condition

$$v(S, 0) = \max(S_T - X, 0), \tag{40}$$

and boundary conditions

$$\begin{aligned} &v(0,\tau) = 0, \\ &v(S,\tau) = S\mathrm{e}^{-q\tau} - X\mathrm{e}^{-r\tau} \quad \text{as } S \to \infty, \end{aligned} \tag{41}$$

where S_T is the stock price at expiration date T. The analytic pricing formula of the European option is available, see Appendix B. The valuation of ECND can be viewed as a special case of the valuation of ECCD with $q = 0$. Thus two types of options can be evaluated by the same procedure. However, there are some minor differences when the underlying asset pays discrete dividends. For simplicity, we only consider the single discrete dividend paying case for European call valuation. At the known ex-dividend date τ_d, the asset price must be reduced by the amount of the dividend D to eliminate riskless arbitrage opportunities

$$S(\tau_d^+) = S(\tau_d^-) + D, \tag{42}$$

where superscripts + and − denote the instants after and before τ_d, respectively. For the valuation of ECDD, the asset price is usually assumed to be made up with two components: a riskless component that corresponds to the known dividend during the life of the option and a risky component ([25], Section 2.2.1). The value of the risky component $\tilde{S}$ is given by

$$\tilde{S} = \begin{cases} S & \text{for } 0 \leqslant \tau \leqslant \tau_d^-, \\ S - D\mathrm{e}^{-r(\tau-\tau_d)} & \text{for } \tau_d^+ \leqslant \tau \leqslant T. \end{cases} \tag{43}$$

When the option matures, the dividend will have been paid and the riskless component will no longer exist. Therefore, to evaluate the option price, one can apply the Black–Scholes formula by taking underlying asset as $\tilde{S}$ and volatility as the one of the risky component $\tilde{S}$. Theoretically, the volatility of the risky component is different from the volatility of the whole stock price. However, in practice, they are often treated as being the same. We will also treat them equally for simplicity. Obviously, after this simplification, the ECDD valuation is essentially equivalent to the ECND valuation.

In the present study, the dividend yield ratio is chosen as $q = 0.02$ for ECCD. The dollar dividend amount is $D = 1$ for ECDD, and the ex-dividend dates are 0.5, 2, and 3.5 months for maturities $T = 1$, 4, and 7 months, respectively. The European option values are estimated by using both the DSC and FD schemes in association with the same uniform stock price-time mesh. The approximation errors and the execution time are given in Table 1. As can be seen from Table 1, in every case, the approximation error of the DSC approach is smaller than that of the FD scheme. However, the difference between them is moderate. That is because, although theoretically the error incurred in a higher-order scheme is usually significantly less than that of a lower-order scheme, numerically the higher-order scheme also has difficulty in capturing the dramatically changing

Table 1
Comparison of European call option valuation by using the DSC and the FD based on a normal mesh

Case	Scheme	$T = 1$		$T = 4$		$T = 7$		ET
		L_∞	L_2	L_∞	L_2	L_∞	L_2	
ECND	EFD	3.10(−3)	5.02(−4)	1.54(−3)	3.51(−4)	1.15(−3)	2.99(−4)	4.74(−4)
	CN	3.20(−3)	5.14(−4)	1.58(−3)	3.60(−4)	1.19(−3)	3.11(−4)	1.40(−3)
	LK	2.13(−3)	3.95(−4)	1.05(−3)	2.76(−4)	7.83(−4)	2.38(−4)	5.08(−2)
	RSK	2.13(−3)	3.95(−4)	1.05(−3)	2.76(−4)	7.83(−4)	2.38(−4)	4.85(−2)
ECCD	EFD	3.09(−3)	5.01(−4)	1.52(−3)	3.49(−4)	1.13(−3)	2.99(−4)	4.74(−4)
	CN	3.19(−3)	5.13(−4)	1.57(−3)	3.58(−4)	1.17(−3)	3.07(−4)	1.40(−3)
	LK	2.13(−3)	3.95(−4)	1.05(−3)	2.77(−4)	7.83(−4)	2.39(−4)	5.11(−2)
	RSK	2.13(−3)	3.95(−4)	1.05(−3)	2.77(−4)	7.83(−4)	2.39(−4)	4.89(−2)
ECCD	EFD	3.05(−3)	4.92(−4)	1.43(−3)	3.25(−4)	1.02(−3)	2.64(−4)	4.74(−4)
	CN	3.14(−3)	5.04(−4)	1.48(−3)	3.34(−4)	1.06(−3)	2.72(−4)	1.42(−3)
	LK	2.07(−3)	3.85(−4)	9.47(−4)	2.49(−4)	6.51(−4)	1.98(−4)	5.26(−2)
	RSK	2.07(−3)	3.85(−4)	9.47(−4)	2.49(−4)	6.51(−4)	1.98(−4)	4.99(−2)

solution in critical regions. On such occasions, a higher-order scheme cannot be superior to a lower-order scheme in terms of accuracy based on a normal uniform mesh. In fact, higher-order schemes are rarely used for the solution of the Black–Scholes equation in the finance literature.

Fortunately, when a higher-resolution grid is employed to capture the dramatic changes of the solution on a small critical region, the discretization error of this high gradient region can be significantly reduced. For European option pricing, several adaptive higher-resolution grids are employed on a small critical region around the strike price X immediately before expiration, each from $S^l_{\min}$ to $S^l_{\max}$ with a spacing ΔS^l and from $\tau = \tau^l_s$ to $\tau = \tau^l_e$ with a time increment $\Delta\tau^l$, $l = 1,2,3,\ldots$, see Fig. 1. Usually, to make sure that the valuation information is transmitted properly, the finer mesh is used with a stock price spacing $\Delta S^l = \Delta S^{l+1}/m$ and a corresponding time increment $\Delta\tau^l = \Delta\tau^{l+1}/m^2 (m \in \mathbb{Z}^+)$. It is noted that the boundary conditions (41) are approximated as

$$\begin{aligned} &v(S^l_{\min}, \tau) = 0, \\ &v(S^l_{\max}, \tau) = S^l_{\max} e^{-q\tau} - X e^{-r\tau}. \end{aligned} \tag{44}$$

When $\tau = \tau^l_e$ is very small, $S^l_{\max}$ and $S^l_{\min}$ can actually be chosen to be much smaller than $S_{\max}$ and bigger than zero, respectively. Such values are already large or small enough to ensure that the call will be almost certainly exercised, or expired out-of-the-money. This tightened boundary condition makes sure that the resolution of critical region is sufficiently high and the additional computation of the adaptive mesh is relatively small. Moreover, by using approximation (44), there is only one grid which needs to be treated at any moment of

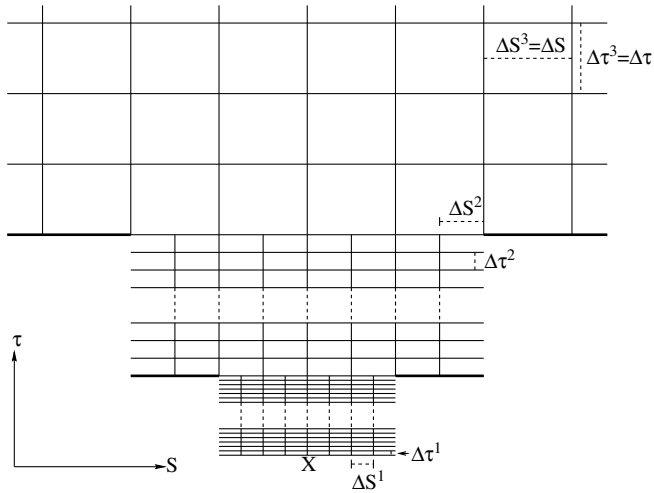

Fig. 1. An illustration of the adaptive mesh employed in the European option valuation problems. Here $l = 2$ and $m = 2$.

computation, so that the algorithm is relatively simple. It is also noted that at the instants $\tau = \tau_e^l$, for $l = 1, 2, 3, \ldots$, the option values of the asset prices which lie outside of the previous computational domain (the parts represented by the bold lines in Fig. 1) can also be directly given by Eq. (44).

In the present computation, we use a total of four sets of grids, i.e., three finer grids and a coarse grid. The total evolution time on all the finer grids is 1/100 month. When $\tau > 1/100$ month, the coarse uniform grid is used. The detailed description of the adaptive mesh employed in European option valuation is given in Table 2. It is noted that the computation on finer grids only carries for a very short time interval, 1/100 month, which is just the last few hours of trading from a practice point of view. Consequently, the present algorithm is able to deal with short-dated options, which are the most popularly traded options.

Based on the same adaptive mesh, the values of European options are approximated via both the DSC and FD again, see Table 3. It is clear from Table 3 that the higher-order scheme gives much higher accuracy than that of the lower-order scheme based on an adaptive mesh. The high resolution grid

Table 2
The adaptive higher-resolution mesh employed in the European option valuation

l	$S_{\min}^l$	$S_{\max}^l$	ΔS^l	τ_s^l	τ_e^l	$\Delta\tau^l$
1	44.5	45.5	2.5(−3)	0.0	5.0(−4)	3.125(−7)
2	44.0	46.0	5.0(−3)	5.0(−4)	1.0(−3)	1.25(−6)
3	40.0	50.0	2.5(−2)	1.0(−3)	1.0(−2)	3.125(−5)

Table 3
Comparison of European call option valuation by using the DSC, the FD, the PP and the SMO

Case	Scheme	$T = 1$		$T = 4$		$T = 7$		ET
		L_∞	L_2	L_∞	L_2	L_∞	L_2	
ECND	EFD	8.20(−4)	1.32(−4)	4.72(−4)	1.06(−4)	3.65(−4)	9.40(−5)	9.48(−4)
	CN	1.06(−3)	1.70(−4)	5.36(−4)	1.21(−4)	4.08(−4)	1.05(−4)	3.39(−3)
	LK	6.11(−8)	1.13(−8)	2.98(−8)	7.85(−9)	2.22(−8)	6.82(−9)	1.31(−1)
	RSK	6.11(−8)	1.13(−8)	2.98(−8)	7.83(−9)	2.22(−8)	6.73(−9)	1.24(−1)
	SMO	2.45(−4)	6.01(−5)	5.06(−4)	1.72(−4)	6.80(−4)	2.64(−4)	4.71(−2)
	SMO_extra	7.06(−8)	1.49(−8)	1.55(−7)	4.67(−8)	2.16(−7)	7.76(−8)	2.36(−1)
	PP	1.98(−8)	3.52(−9)	3.90(−8)	1.01(−8)	5.07(−8)	1.56(−8)	4.67(−2)
	PP_extra	1.04(−8)	1.77(−9)	1.96(−8)	5.04(−9)	2.54(−8)	7.78(−9)	2.37(−1)
ECCD	EFD	8.16(−4)	1.31(−4)	4.63(−4)	1.05(−4)	3.55(−4)	9.22(−5)	9.23(−4)
	CN	1.05(−3)	1.70(−4)	5.29(−4)	1.20(−4)	3.98(−4)	1.03(−4)	3.39(−3)
	LK	6.11(−8)	1.13(−8)	2.98(−8)	7.88(−9)	2.22(−8)	6.86(−9)	1.29(−1)
	RSK	6.11(−8)	1.13(−8)	2.98(−8)	7.86(−9)	2.22(−8)	6.78(−9)	1.24(−1)
ECDD	EFD	8.20(−4)	1.32(−4)	4.72(−4)	1.06(−4)	3.65(−4)	9.40(−5)	9.98(−4)
	CN	1.06(−3)	1.70(−4)	5.36(−4)	1.21(−4)	4.08(−4)	1.05(−4)	3.37(−3)
	LK	1.26(−7)	3.45(−8)	8.75(−9)	6.04(−9)	5.30(−8)	1.87(−8)	1.30(−1)
	RSK	1.26(−7)	3.45(−8)	7.36(−9)	5.61(−9)	5.30(−8)	1.82(−8)	1.25(−1)

Here _extra denotes that the extrapolation technique is used.

in the critical region enables the scheme to capture the rapid changes of the option price. At the region of the low resolution grid, since the changes in option price are relatively slow, the higher-order scheme yields very accurate approximations. However, for the lower-order scheme, the discretization error at the region of the low resolution grid is still large, hence, the significance of utilizing adaptive mesh is cancelled out. We further illustrate this observation by estimating the European option values only based on the coarse grid region, i.e. input the exact Black–Scholes option value to each stock price node at $\tau = 1/100$ month and calculate until it matures by using a coarse uniform mesh (the similar techniques for binomial tree method refer to [9,16]). The results are listed in Table 4, which agree with the aforementioned theoretical analysis.

For non-dividend paying case, two lattice approaches are also employed to evaluate the European option price. The results are also contained in Table 3. Here time refinements are chosen as 2000 and 2001 for SMO and PP models, respectively. The corresponding time increment of two lattice approaches in pricing options with one month maturity is the same as (or approximately equal to) that used in PDE methods on the normal mesh. Highly accurate results are obtained by using the PP model. The extrapolation technique is also used for both models, with much larger time refinements, i.e., 4000 and 4001 for SMO and PP, respectively. Much improvement is achieved by using the extrapolation in the SMO results, while the accuracy improvement in PP results is moderate. With a longer execution time, the extrapolation results of

Table 4
Comparison of European call option valuation by using the DSC and the FD

Case	Scheme	$T = 1$		$T = 4$		$T = 7$		ET
		L_∞	L_2	L_∞	L_2	L_∞	L_2	
ECND	EFD	9.60(−4)	1.55(−4)	4.89(−4)	1.10(−4)	3.73(−4)	9.59(−5)	4.49(−4)
	CN	1.06(−3)	1.70(−4)	5.36(−4)	1.21(−4)	4.08(−4)	1.05(−4)	1.37(−3)
	LK	8.31(−9)	1.45(−9)	3.59(−9)	1.16(−9)	3.29(−9)	1.47(−9)	5.04(−2)
	RSK	8.31(−9)	1.44(−9)	3.59(−9)	9.35(−10)	2.62(−9)	7.98(−10)	4.82(−2)
ECCD	EFD	9.57(−4)	1.54(−4)	4.81(−4)	1.09(−4)	3.62(−4)	9.42(−5)	4.49(−4)
	CN	1.05(−3)	1.70(−4)	5.29(−4)	1.20(−4)	3.98(−4)	1.03(−4)	1.37(−3)
	LK	8.35(−9)	1.46(−9)	3.61(−9)	1.16(−9)	3.24(−9)	1.45(−9)	4.97(−2)
	RSK	8.35(−9)	1.45(−9)	3.60(−9)	9.43(−10)	2.64(−9)	8.06(−10)	4.84(−2)
ECDD	EFD	9.60(−4)	1.55(−4)	4.89(−4)	1.10(−4)	3.73(−4)	9.59(−5)	4.49(−4)
	CN	1.06(−4)	1.70(−4)	5.36(−4)	1.21(−4)	4.08(−4)	1.05(−4)	1.40(−3)
	LK	1.60(−8)	4.29(−9)	5.12(−9)	1.92(−9)	5.43(−9)	2.50(−9)	5.21(−2)
	RSK	1.96(−8)	4.30(−9)	4.94(−9)	1.71(−9)	5.10(−9)	1.91(−9)	4.91(−2)

Calculations start at $\tau = \frac{1}{100}$ month.

SMO (PP) model are slightly less (more) accurate than those of the DSC. Generally speaking, both the DSC and two lattice approaches exhibit similarly very high accuracy and are much more efficient than the conventional lower order schemes. It is noted that two lattice approaches were only presented for non-dividend paying cases in the original Refs. [28,26]. Thus, two dividend paying cases are not studied for two lattice approaches in the present paper.

3.1.2. European put option

Due to the put-call parity theorem [25], a European put value can be directly given if the corresponding European call value is known. However, puts do have some properties that differ from calls, such as the possible range of elasticity. To further test the performance of the DSC for European option valuation problem, European puts on continuous dividend paying assets (EPCD) are studied. The results of other two dividend cases are similar to those of EPCD, and are omitted.

The value of a European put can be approximated by numerically solving Eq. (4) subject to the initial condition

$$v(S, 0) = \max(X - S_T, 0), \tag{45}$$

and boundary conditions

$$\begin{aligned} v(S, \tau) &= 0 \qquad \text{as } s \to \infty, \\ v(S, \tau) &= X\mathrm{e}^{-r\tau} \quad \text{as } s \to 0^+. \end{aligned} \tag{46}$$

The dividend yield ratio is chosen as $q = 0.07$ in the present study. The same normal and adaptive meshes as in European call option valuation are used.

Table 5
Comparison of European put option valuation by using the DSC and the FD

Scheme	$T = 1$		$T = 4$		$T = 7$		ET
	L_∞	L_2	L_∞	L_2	L_∞	L_2	
EFD1	3.09(−3)	4.99(−4)	1.50(−3)	3.45(−4)	1.11(−3)	2.93(−4)	4.00(−4)
EFD2	8.16(−4)	1.33(−4)	4.62(−4)	1.10(−4)	3.53(−4)	9.94(−5)	8.75(−4)
CN1	3.18(−3)	5.12(−4)	1.55(−3)	3.54(−4)	1.15(−3)	3.02(−4)	2.35(−3)
CN2	1.05(−3)	1.72(−4)	5.29(−4)	1.25(−4)	3.99(−4)	1.12(−4)	5.95(−3)
LK1	2.12(−3)	3.96(−4)	1.05(−3)	2.79(−4)	7.83(−4)	2.42(−4)	4.91(−2)
LK2	6.13(−8)	1.13(−8)	2.98(−8)	7.94(−9)	2.22(−8)	6.89(−9)	1.30(−1)
RSK1	2.12(−3)	3.96(−4)	1.05(−3)	2.79(−4)	7.83(−4)	2.42(−4)	4.77(−2)
RSK2	6.13(−8)	1.13(−8)	2.98(−8)	7.94(−9)	2.22(−8)	6.89(−9)	1.24(−1)

Scheme 1 is calculated on a normal mesh, while scheme 2 is calculated on an adaptive mesh.

The corresponding DSC and FD results are listed in Table 5. It can seen from Table 5 that the present results are similar to those in European call option valuation. This finding is consistent with that of Geske and Shastri [19]. In summary, under appropriate conditions, the DSC algorithm outperforms the lower-order scheme in terms of accuracy and efficiency for the European option pricing problem.

3.2. American option

As American options can be exercised at any time before expiration, a live American option must be worth at least its intrinsic value. In general, there is a critical value, S^*, of the underlying asset. For a holder of an American option, it makes no difference whether to exercise the option or not at this critical value. The determination of this critical value makes the valuation of American options a free boundary problem. This leads to the following constraint condition:

$$v(S,\tau) \geqslant \begin{cases} \max(S-X,0) & \text{for American call,} \\ \max(X-S,0) & \text{for American put,} \end{cases} \tag{47}$$

which implies

$$v(S^*,\tau) = \begin{cases} \max(S^*-X,0) & \text{for American call,} \\ \max(X-S^*,0) & \text{for American put.} \end{cases} \tag{48}$$

Since the critical value S^* can not be known in advance, we have to impose the free boundary conditions as part of the solution procedure, which introduces considerable difficulties, both theoretically and numerically. Therefore, for American options, analytic valuation formulae are generally not available, except for a few special types, i.e. American calls on non-dividend paying assets (which actually have identical values as ECND) and American calls on discrete

dividend paying assets. Alternatively, approximation approaches have been proposed in the literature. Interested readers may refer to [25] and the references therein.

The American option price function $v(S,\tau)$ satisfies the Black–Scholes equation (4) together with the auxiliary conditions: the constraint (47) and the payoff (40) for a call or (45) for a put. The characteristic of the early exercise feature of American options depends crucially on the dividend payout of the underlying stock (see for example [25]). Consequently, the optimal exercise curve for an American option might be totally different when the underlying asset is non-dividend paying or dividend paying (discrete or continuous). Numerically, different solution procedures should be employed to properly treat different free boundaries. Therefore, three typical valuation problems which have different characteristics of the early exercise feature are studied separately in the present work. These problems include all nontrivial American option valuations.

3.2.1. American calls on discrete dividend paying assets (ACDD)

ACDD will be possibly exercised only at instants immediately prior to the ex-dividend dates. Thus, the ACDD can be replicated by a portfolio of European compound options with the maturity dates of the compound options coinciding with the ex-dividend dates. Consequently, the analytic pricing formula for ACDD can be derived according to such a replication strategy, and is presented in Appendix B.

For simplicity, we only consider the single discrete dividend paying case and the dividend parameters are the same as those in ECDD valuation. Numerically, by denoting $\tilde{S}^*$ as the critical risky asset value, the approximated American call price at instant $\tau = \tau_d^+$ is given by

$$v(\tilde{S}, \tau_d^+) = \begin{cases} \bar{v}(\tilde{S}, \tau_d^-) & \text{when } \tilde{S} < \tilde{S}^*, \\ \tilde{S} - X & \text{when } \tilde{S} \geqslant \tilde{S}^*, \end{cases} \tag{49}$$

where $\bar{v}(\tilde{S}, \tau_d^-)$ is the approximated American call price at instant $\tau = \tau_d^-$. Since the underlying asset does not pay a dividend during $\tau = [0, \tau_d^-]$, $\bar{v}(\tilde{S}, \tau_d^-)$ is actually the corresponding European call price and can be similarly approximated as in European call valuation. For the live American call ($\tilde{S} < \tilde{S}^*$), its value remains unchanged as time passes across the dividend date. For the American call with underlying asset $\tilde{S} > \tilde{S}^*$, it will be exercised at instant τ_d^+ to capture the dividend. Numerically, both kinds of American calls, alive or not, are calculated in the whole computational domain. Except the ex-dividend instant, the computation procedure for ACDD valuation can be the same as that in European call valuation, and the same uniform mesh as in the European case is used. Based on such a uniform mesh, the value of ACDD is approximated by using the DSC and EFD, see Table 6. Similar to the European case, the results of the DSC are only slightly more accurate than those of the EFD.

Table 6
Comparison of ACDD valuation by using the DSC and the EFD

Scheme	$T = 1$		$T = 4$		$T = 7$		ET
	L_∞	L_2	L_∞	L_2	L_∞	L_2	
EFD1	2.07(−3)	2.85(−4)	1.56(−3)	3.47(−4)	1.15(−3)	3.00(−4)	4.00(−4)
EFD2	1.21(−3)	1.70(−4)	5.39(−4)	1.15(−4)	3.78(−4)	9.50(−5)	4.06(−2)
LK1	1.04(−3)	1.64(−4)	1.00(−3)	2.48(−4)	7.57(−4)	2.19(−4)	5.05(−2)
LK2	4.96(−8)	7.30(−9)	5.58(−8)	1.25(−8)	1.91(−8)	5.66(−9)	3.41(−1)
RSK1	1.04(−3)	1.64(−4)	1.00(−3)	2.48(−4)	7.57(−4)	2.19(−4)	4.72(−2)
RSK2	4.96(−8)	7.30(−9)	1.46(−8)	3.69(−9)	1.91(−8)	5.63(−9)	3.39(−1)

Scheme 1 is calculated on a normal mesh, while scheme 2 is calculated on an adaptive mesh.

To achieve more accurate results, a suitable adaptive mesh is indispensable. However, the appropriate adaptive mesh for ACDD is different from the one used in the European case, since apart from the critical region around strike price, there is another critical region around $\tilde{S}^*$ before ex-dividend. Before dividend paying, there will be no dividend paying from $\tau = \tau_d^+$ to $\tau = T$. Hence, the problem becomes an ECND valuation one with time to expire $T - \tau_d^+$ and initial pay-off function $v(\tilde{S}, \tau_d^+)$, which is given by Eq. (49). Similar to the European option valuation, this pay-off function is not differentiable, because at critical asset price $\tilde{S}^*$, the approximated European call (i.e. $\bar{v}(\tilde{S}, \tau_d^-)$) price curve intersects (not tangentially) the early exercise line, $\tilde{S} - X$. Consequently, option value will undergo sharp changes around $\tilde{S}^*$ before ex-dividend. The discretization of this critical region can also induce very serious pricing errors. Hence, apart from the adaptive region as that used in European valuation problems, another higher-resolution region is also employed (from $\tilde{S}^d_{\min}$ to $\tilde{S}^d_{\max}$ with a spacing $\Delta\tilde{S}^d$ and from τ_d to $\tau_d + 1/100$ with a time increment $\Delta\tau^d$). When $\tau \in (\tau_d, \tau_d + 1/100]$, calculations are carried out on a higher-resolution mesh and a lower-resolution mesh simultaneously. The detailed description of the adaptive mesh is given in Table 7, and an illustrative graph is given in Fig. 2.

To initiate the adaptive mesh computation, an off-grid interpolation is required. It is interesting to note that the DSC algorithm also provides highly accurate interpolations (set $n = 0$ in the Eq. (24)). Such interpolation is used

Table 7
The higher resolution mesh employed in ACDD valuation around the critical asset price

τ_d	$\tilde{S}^d_{\min}$	$\tilde{S}^d_{\max}$	$\Delta\tilde{S}^d$	$\Delta\tau^d$
0.5	$[\tilde{S}^*] - 2.0$	$[\tilde{S}^*] + 2.5$	1.0(−2)	2.0(−7)
2.0	$[\tilde{S}^*] - 2.5$	$[\tilde{S}^*] + 2.5$	1.25(−2)	3.125(−7)
3.5	$[\tilde{S}^*] - 3.0$	$[\tilde{S}^*] + 2.0$	1.25(−2)	3.125(−7)

Here $[\tilde{S}^*]$ denotes the asset node on the coarse grid, which has the smallest distance departed from the critical price $\tilde{S}^*$ among all coarse grid nodes.

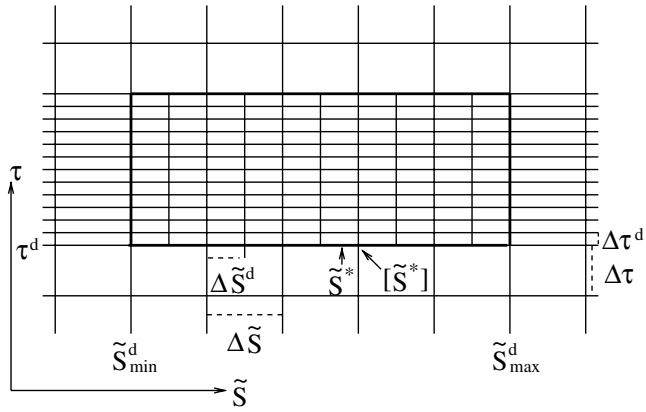

Fig. 2. An illustration of the adaptive mesh employed in the ACDD pricing problems immediately prior to the ex-dividend date. The critical region is marked by the bold lines in the figure.

in both the DSC and FD algorithms. Unlike the European counterpart, the boundary conditions for the second critical region is relevantly difficult to handle. The boundary condition at $\tilde{S} = \tilde{S}^d_{\max}$ can be approximated as

$$v(\tilde{S}^d_{\max}, \tau) = \tilde{S}^d_{\max} - X. \tag{50}$$

However, the explicit expression of the boundary condition imposed at $\tilde{S} = \tilde{S}^d_{\min}$ is unavailable. Numerically, to advance to next time step, the derivative values of price at some nodes, which lie in the critical region and close to $\tilde{S} = \tilde{S}^d_{\min}$, are required to be known. In the present computation, those derivative values are explicitly approximated, which involves certain points outside the left boundary of critical region. The values on those points are interpolated from the option values on the lower-resolution mesh at each time step. Consequently, to ensure a high accuracy, the option values calculated on the lower-resolution mesh are corrected by those on the higher-resolution mesh, after each time increment. Again, the DSC interpolation is used both in the DSC and FD algorithms. Quite satisfactory accuracy can be obtained by using this boundary treatment, provided that the lasting time length of the higher-resolution mesh is sufficiently small, such as 1/100 month here. However, it is relevantly difficult to implement such boundary treatment within an implicit time-stepping scheme. Therefore, for simplicity, we do not consider the CN scheme in the ACDD valuation. The approximation errors and execution time, obtained by using the DSC and EFD algorithms in association with the adaptive mesh, are also presented in Table 6. Similar to European cases, significant improvement is achieved in the DSC results, while the improvement in the EFD results is very small. These results indicate that the DSC approach works extremely well in pricing the American option.

3.2.2. Continuous optimal exercise boundaries

American calls on continuous dividend paying assets (ACCD), American puts on continuous dividend paying assets (APCD), and American puts on non-dividend paying assets (APND) have similar optimal exercise boundaries. The optimal exercise boundaries exist at any living time, and are monotonic and continuous functions of time. Furthermore, there is a common feature for the optimal exercise boundary of these three cases, i.e., both the option value v and its derivative $\partial v/\partial S$ are continuous across the optimal exercise boundary, which is known as the high contact condition in the finance literature. In particular, if we denote the optimal exercise boundary by $S^*(\tau)$, the value of these three types of American options can be determined by solving Eq. (4) subject to the payoff condition (40) and free boundary conditions

$$\begin{aligned} &S^*(0) = \max(X, rX/q), \\ &v(0,\tau) = 0, \\ &v(S^*(\tau),\tau) = S^*(\tau) - X, \end{aligned} \tag{51}$$

for calls or conditions (45) and

$$\begin{aligned} &S^*(0) = \min(X, rX/q), \\ &v(S,\tau) = 0 \text{ as } S \to \infty, \\ &v(S^*(\tau),\tau) = X - S^*(\tau), \end{aligned} \tag{52}$$

for puts, respectively.

Numerically, the free boundary conditions can be approximated by means of Eq. (47) as [7,19]

$$v_i^j = \begin{cases} \max(S_i - X, \bar{v}_i^j, 0) & \text{for American call option,} \\ \max(X - S_i, \bar{v}_i^j, 0) & \text{for American put option,} \end{cases} \tag{53}$$

where $v_i^j = v(i\Delta S, j\Delta\tau)$, and $\bar{v}_i^j$ is the value directly calculated from the last time step $j-1$ based on the discretized form of Eq. (4). The time discretization error of (53) is of first order, thus the Runge–Kutta method is replaced by the explicit Euler method, Eq. (32), in the DSC algorithm for time-stepping. In other words, for both the DSC and EFD schemes, the same temporal discretization is employed, and the time-stepping error is of first order.

No closed form valuation formula exists for these three types of options. The accuracy of the numerical approximation is commonly assessed by a comparison with benchmark values estimated by using the binomial tree method [9]. In the present study, we first evaluate the European counterparts of these three types of options by using the binomial tree method with very large time refinements. The binomial model parameters used are those of [20,9]. The results are given in Table 8. We then estimate the benchmark values of these three types of American options by using the binomial tree method and with

Table 8
European option valuation by using the binomial tree method

Case	T	N_{bt}	L_∞	L_2	ET
EPND	1	124001	8.66(−6)	1.56(−6)	1.23(+2)
	4	248001	7.97(−6)	2.20(−6)	4.97(+2)
	7	320001	7.75(−6)	2.81(−6)	1.13(+3)
EPCD	1	124001	9.60(−6)	1.64(−6)	1.64(+2)
	4	248001	9.56(−6)	2.34(−6)	9.05(+2)
	7	320001	9.66(−6)	3.04(−6)	1.82(+3)
ECCD	1	124001	9.82(−6)	1.69(−6)	1.24(+2)
	4	248001	1.02(−5)	2.50(−6)	9.18(+2)
	7	320001	1.06(−5)	3.33(−6)	1.16(+3)

N_{bt} denotes the total number of time refinement used in the binomial tree method. EPND denotes the European put on non-dividend paying assets.

the same time refinements as in Table 8. Therefore, the approximation errors in Table 8 provide the accuracy level of these benchmark values. It should be emphasized that the execution time in Table 8 is very large. Moreover, the execution time of American option valuation via the binomial tree method is even larger than (1.82–3.58 times of) that of the European case. This gives an inkling on how expensive the computational cost would be by using a lower-order approximation scheme to achieve a satisfactory accuracy.

The values of three options are approximated by using the DSC and EFD schemes based on the same uniform mesh, see Table 9. In general, the DSC results are more accurate than those of the EFD. For the present American option valuation problem, it is generally very difficult to design a fully adaptive mesh which can well control the discretization error. Although a high contact condition holds at the optimal exercise boundary, the gamma values of the option prices are discontinuous on the optimal exercise boundary. Thus, the discretization errors along the free boundary are relatively large and may affect the final accuracy. On the other hand, the optimal exercise boundary is unknown in advance and exists during the whole life of options, so that the efficiency of using a higher-resolution grid at the critical region of the optimal exercise boundary is relatively low. Therefore, for simplicity, we just use a relatively finer grid in the whole domain (an even finer grid is employed from $\tau = T - 1$ to $\tau = T$) and only one adaptive region is used around the strike price as in the European case. It is noted that, since the $S^*(0)$ may be different from X (Eqs. (51) and (52)), the critical region generally has to include more asset price nodes than the European case. In the present study, more difficult model parameters are selected, i.e., $q = 0.02$ for ACCD and $q = 0.07$ for APCD, while other model parameters are unchanged. Consequently, the boundary of the critical region must satisfy $[S^l_{\min}, S^l_{\max}] \supset [45, 112.5]$ and $[S^l_{\min}, S^l_{\max}] \supset [32.14, 45]$ for calls and puts, respectively. Corresponding, in order to avoid a large computational burden,

Table 9
Comparison of APND, APCD, and ACCD valuation by using the DSC, the EFD, the PP and the SMO

Case	Scheme	$T = 1$		$T = 4$		$T = 7$		ET
		L_∞	L_2	L_∞	L_2	L_∞	L_2	
APND	EFD1	3.43(−3)	6.81(−4)	1.80(−3)	5.08(−4)	1.38(−3)	4.40(−4)	7.12(−4)
	EFD2	2.77(−4)	5.69(−5)	2.22(−4)	6.26(−5)	1.91(−4)	5.98(−5)	9.42(−3)
	LK1	1.67(−3)	3.72(−4)	7.56(−4)	2.36(−4)	5.35(−4)	1.94(−4)	7.30(−3)
	LK2	1.00(−5)	2.24(−6)	6.39(−6)	2.56(−6)	8.10(−6)	2.97(−6)	9.95(−2)
	RSK1	1.64(−3)	3.65(−4)	7.42(−4)	2.32(−4)	5.26(−4)	1.91(−4)	6.48(−3)
	RSK2	1.00(−5)	2.23(−6)	6.36(−6)	2.54(−6)	8.03(−6)	2.95(−6)	9.38(−2)
APCD	EFD1	3.09(−3)	5.98(−4)	1.51(−3)	4.13(−4)	1.11(−3)	3.52(−4)	7.12(−4)
	EFD2	2.43(−4)	5.01(−5)	1.17(−4)	3.43(−5)	8.94(−5)	3.01(−5)	9.96(−3)
	LK1	1.92(−3)	4.47(−4)	9.88(−4)	3.24(−4)	7.46(−4)	2.83(−4)	7.30(−3)
	LK2	1.47(−5)	3.99(−6)	8.77(−6)	3.99(−6)	8.32(−6)	4.18(−6)	1.05(−1)
	RSK1	1.92(−3)	4.48(−4)	9.94(−4)	3.26(−4)	7.51(−4)	2.85(−4)	6.48(−3)
	RSK2	1.47(−5)	4.00(−6)	8.79(−6)	4.00(−6)	8.34(−6)	4.20(−6)	9.98(−2)
ACCD	EFD1	3.10(−3)	5.99(−4)	1.53(−3)	4.19(−4)	1.14(−3)	3.60(−4)	7.12(−4)
	EFD2	2.44(−4)	4.60(−5)	1.31(−4)	3.41(−5)	9.68(−5)	2.86(−5)	1.31(−2)
	LK1	2.03(−3)	5.24(−4)	1.13(−3)	4.26(−4)	9.02(−4)	3.90(−4)	7.30(−3)
	LK2	1.54(−5)	4.01(−6)	9.93(−6)	3.56(−6)	8.54(−6)	3.62(−6)	1.33(−1)
	RSK1	2.03(−3)	5.44(−4)	1.17(−3)	4.52(−4)	9.41(−4)	4.16(−4)	6.58(−3)
	RSK2	1.59(−5)	4.13(−6)	1.03(−5)	3.71(−6)	8.88(−6)	3.77(−6)	1.29(−1)

Scheme 1 is calculated on the same normal mesh, while scheme 2 is calculated on the same adaptive mesh.

the highest resolution in the critical region is much lower than that used in the European option valuation, see Table 10.

Table 10
The adaptive higher-resolution mesh employed in valuation of APND, APCD, and ACCD

Case	l	$S^l_{\min}$	$S^l_{\max}$	ΔS^l	τ^l_s	τ^l_e	$\Delta\tau^l$
APND	1	42.5	47.5	2.5(−2)	0.0	5.0(−3)	1.25(−6)
	2	40.0	50.0	5.0(−2)	5.0(−3)	5.0(−2)	5.0(−6)
	3	0.0	140.0	2.5(−1)	5.0(−2)	6.0	1.25(−4)
	4	0.0	140.0	1.25(−1)	6.0	7.0	3.125(−5)
APCD	1	31.5	46.5	2.5(−2)	0.0	5.0(−3)	1.25(−6)
	2	30.0	50.0	5.0(−2)	5.0(−3)	5.0(−2)	5.0(−6)
	3	0.0	140.0	2.5(−1)	5.0(−2)	6.0	1.25(−4)
	4	0.0	140.0	1.25(−1)	6.0	7.0	3.125(−5)
ACCD	1	42.5	114.5	2.5(−2)	0.0	5.0(−3)	1.25(−6)
	2	40.0	120.0	5.0(−2)	5.0(−3)	5.0(−2)	5.0(−6)
	3	0.0	140.0	2.5(−1)	5.0(−2)	6.0	1.25(−4)
	4	0.0	140.0	1.25(−1)	6.0	7.0	3.125(−5)

In three cases above, the maturity time is $T = 7$ months. For other maturity times, the mesh can be constructed in the similar manner.

The approximation errors and the execution time of the DSC and EFD schemes in association with the same adaptive mesh are also listed in Table 9. As can be seen from Table 9, for both the DSC and FD, the execution time roughly increases 15 times after using the adaptive mesh. At the same time, by using the adaptive mesh, the DSC and the EFD results are round 100 and 10 times more accurate than those obtained by using the normal mesh, respectively. The improvement of accuracy is dramatically high in the DSC results, while it is moderate in the EFD results. The accuracy of the DSC results is actually the same as the benchmark values. However, the DSC algorithm is much faster than the traditional binomial tree method, see both Tables 8 and 9. In particular, The execution time of the traditional binomial tree method is from 18270 to 35238 times larger than that of the DSC algorithm. This reveals that in terms of accuracy and efficiency, the DSC approach remarkably outperforms the conventional lower-order schemes.

To investigate the spatial discretization error of both the DSC and EFD schemes in depth, a numerical convergence test is performed. For simplicity, we focus ourselves on the valuation of APND with $T = 7$ month. By keeping $\Delta\tau^l$ very small and unchanged, we refine the entire adaptive mesh twice. The option prices approximated by both the DSC and FD at the strike ($S = 45$) are presented in Table 11. The numerically tested spatial discretization order of the DSC scheme for American option valuation is higher than that of the EFD scheme, however, they all are just second order convergence. The reason for the low displayed order of the DSC scheme is due to the complicate nature of numerical American option valuation problem. In particular, the gamma of option prices is discontinuous which reduces the accuracy of the DSC scheme.

Table 11
APND valuation based on different adaptive meshes

Scheme	Mesh	Value	Change	Ratio	ET
DSC	1	0.20893750			1.96
	2	0.20894109	3.59(−6)		4.47
	3	0.20894181	7.19(−7)	4.99	7.45
EFD	1	0.20903803			2.06(−1)
	2	0.20896591	7.21(−5)		3.74(−1)
	3	0.20894799	1.79(−5)	4.03	8.49(−1)

Here in mesh 1, 2, and 3, $S^l_{\min}$, $S^l_{\max}$, τ^l_s, and τ^l_e are the same in Table 10. The time increments of three adaptive meshes are the same and are 10 times smaller than those listed in Table 10, i.e. $\Delta\tau^1 = 1.25(-7)$, $\Delta\tau^2 = 5.0(-7)$, $\Delta\tau^3 = 1.25(-5)$, and $\Delta\tau^4 = 3.125(-6)$. The spacing sizes ΔS^l of mesh 2 are the same as those given in Table 10, while the spacing sizes of mesh 1 and 3 are half and twice of those of mesh 2, respectively. Change is the difference in the solution from the coarser mesh. Ratio is the ratio of the change on successive meshes.

Table 12
The APND valuation by using the PP and the SMO approaches

Scheme	$T = 1$		$T = 4$		$T = 7$		ET
	L_∞	L_2	L_∞	L_2	L_∞	L_2	
SMO	2.25(−4)	5.99(−5)	4.34(−4)	1.56(−4)	5.69(−4)	2.32(−4)	1.14(−1)
SMO_extra	9.00(−6)	1.45(−6)	1.69(−5)	2.10(−6)	4.02(−5)	3.66(−6)	6.18(−1)
PP	3.56(−5)	5.46(−6)	1.21(−4)	2.29(−5)	1.87(−4)	4.03(−5)	1.15(−1)
PP_extra	8.98(−6)	1.45(−6)	1.65(−5)	2.08(−6)	4.38(−5)	3.77(−6)	6.18(−1)

Here _extra denotes that the extrapolation technique is used. The time refinements used in the SMO and PP models are the same as those used in European call valuation.

Although having the similar convergence order, the DSC does have much smaller approximation error than the EFD scheme. For example, in Table 9, the DSC results are generally 10 times more accurate than those of the EFD scheme. Since the execution time of the EFD scheme is only 10 times faster than that of the DSC algorithm, to achieve the same accuracy level of the DSC, it would consume longer computational time than the DSC scheme. To give an example calculation, we also consider the APND with $T = 7$ month. By using an adaptive mesh with twicely refined resolutions (i.e. $\Delta S'/4$ and $\Delta\tau'/16$) as those reported in Table 10, the EFD results have the errors: $L_\infty = 1.84(-5)$ and $L_2 = 5.77(-6)$. These errors are still larger than those of the DSC results reported in Table 9, while the execution time of the EFD scheme now is 6.45(−1) second, which is 6.5 times of that of the LK scheme. In summary, the DSC scheme performs better than the low accuracy FD scheme for the American option valuation.

In order to compare the DSC with other higher order numerical methods, the APND values are also approximated by the SMO and PP models, see Table 12. The time refinements of two models are keeping the same as those in ECND valuation. Similar to the European case, after extrapolation, very accurate results are obtained for both lattice approaches, which are at the same accuracy level as the DSC results. However, the execution time now is much larger than that of the DSC results. In terms of efficiency, the DSC scheme is better than two higher order lattice approaches for the American option valuation.

3.2.3. American puts on discrete dividend paying assets (APDD)

The optimal exercise boundary of APDD is very irregular and complicated. The numerical valuation of APDD is rarely reported in the finance literature, partly because of the computational difficulty of tracking the optimal exercise boundary. Although no analytic valuation formula exists for APDD, some general behaviors of the optimal exercise boundary $S^*(\tau)$ are known (see [25], Section 4.1.6). Let us consider the single dividend case first. The optimal

exercise boundary is closely related to the competition between the interest income, $X[e^{r(\tau-\tau_d)}-1]$, and the discrete dividend, D. For example, when $X[e^{r(\tau-\tau_d)}-1] < D$, the benefit from the asset price decline of amount D is more attractive than the interest income gained, so that early exercise is not optimal. In general, there exists a critical value τ_d^*, such that

$$X[e^{r(\tau_d^*-\tau_d)}-1] = D. \tag{54}$$

This gives

$$\tau_d^* = \tau_d + \frac{1}{r}\ln\left(1+\frac{D}{X}\right). \tag{55}$$

Within the interval $[\tau_d, \tau_d^*]$, the holder will not exercise the put no matter how low the asset price attains, since $X[e^{r(\tau-\tau_d)}-1] \leqslant D$. When $\tau > \tau_d^*$ (now $X[e^{r(\tau-\tau_d)}-1] > D$), early exercise may become optimal provided that the put is sufficiently deep in-the-money. The similarly properties hold for multi dividend case, such as three dividend case considered here. With dividend amount D_1, D_2, and D_3, and ex-dividend dates τ_1, τ_2, and τ_3, we have $S^*(\tau) = 0$ for $\tau \in (\tau_j, \tau_j^*]$, $j = 1,2,3$. Here critical values τ_j^* can be also analytically given by

$$\tau_j^* = \tau_j + \frac{1}{r}\ln\left(1+\frac{D_j}{X}\right), \quad j = 1,2,3. \tag{56}$$

In the present numerical study, τ_j^* is used as the benchmark for evaluating numerical results. For simplicity, we only consider the DSC algorithm with RSK kernel for this problem. The numerical results, obtained by using the DSC algorithm in association with normal uniform meshes of different

Table 13
The numerical simulation results of APDD by using the DSC

Case	ΔS	$\Delta\tau$	τ_j^*	$\hat{\tau}_j^*$	L_∞	ET
1	0.5	6.25(−4)	6.151960685	6.151875000	8.57(−5)	6.80(−3)
	0.25	1.5625(−4)	6.151960685	6.151875000	8.57(−5)	2.75(−2)
	0.125	3.90625(−5)	6.151960685	6.151953125	7.56(−6)	1.10(−1)
2	0.25	1.5625(−4)	1.829643397	1.829531250	1.12(−4)	2.78(−2)
			5.329643396	5.329531250		
	0.125	3.90625(−5)	1.829643397	1.829609375	3.40(−5)	1.11(−1)
			5.329643396	5.329609375		
3	0.125	3.90625(−5)	0.915742505	0.915742187	3.18(−7)	1.11(−1)
			4.165742505	4.165742187		
			5.665742505	5.665742187		

Cases 1, 2 and 3 represent that the underlying asset pays 1, 2 and 3 discrete dividend, respectively. In all the three cases, $T = 7$ months. In case 1, $D_1 = 0.5$ and $\tau_1 = 3.5$ months; In case 2, $D_1 = D_2 = 0.25$, $\tau_1 = 0.5$ and $\tau_2 = 4.0$ months; In case 3, $D_1 = D_2 = D_3 = 0.125$, $\tau_1 = 0.25$, $\tau_2 = 3.5$ and $\tau_3 = 5.0$ months.

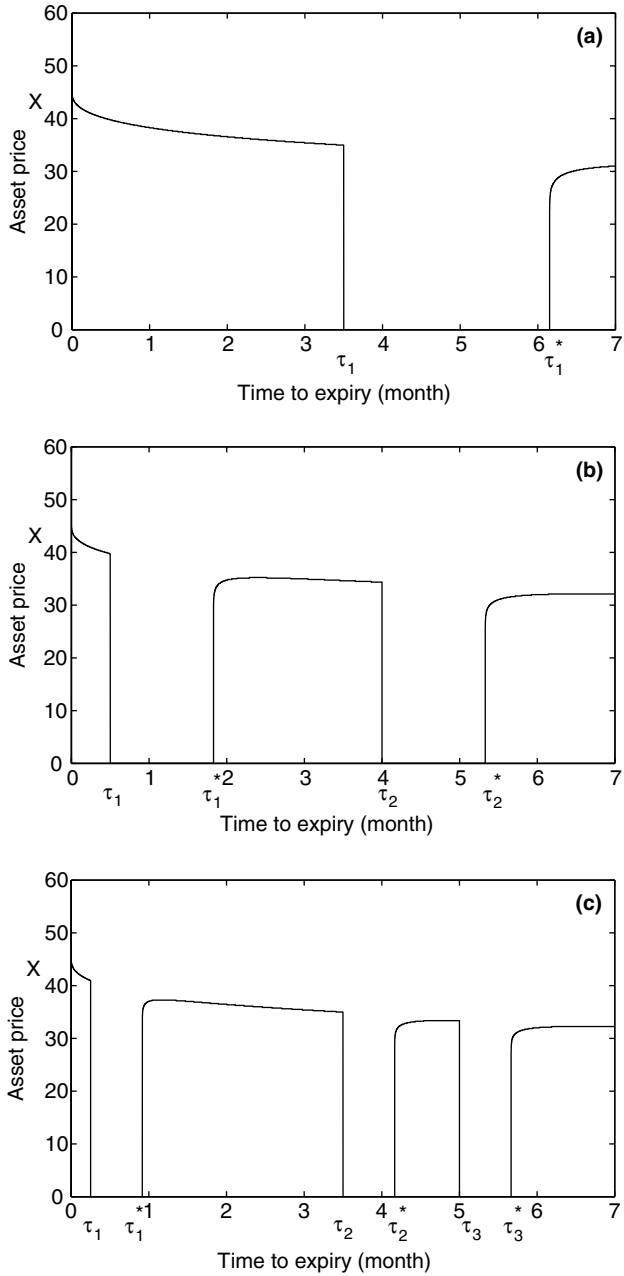

Fig. 3. The simulated behavior of the optimal exercise boundary $S^*(\tau)$ as a function of τ for APDD. (a) one dividend model; (b) two dividend model; (c) three dividend model. The model parameters are the same as those in Table 13.

resolutions, are assessed by a comparison of the estimated $\hat{\tau}_j^*$ with the analytic value τ_j^*, see Table 13. The estimated optimal exercise boundaries are shown in Fig. 3. These numerical results agree very well with the theoretical analysis, which means that the DSC approach is robust and accurate for the American option valuation.

4. Conclusion

This paper explores the utility of the discrete singular convolution (DSC) algorithm for solving the Black–Scholes equation. DSC kernels of Shannon and Lagrange are employed for this application. Two classes of financial option valuation problems, which cover all nontrivial plain option pricing problems, are utilized to illustrate the robustness and accuracy of the present approach. All the DSC results are validated either by the analytical solution or by the binomial tree method. Extensive comparisons are carried out with two high accuracy lattice approaches and two standard finite difference FD schemes.

The first class of problems is European option valuation. Three different dividend payout cases, non-dividend, continuous dividend, and discrete dividend cases, are employed to test the present approach. The results are more accurate than those obtained by using FD schemes. The detailed investigation on the generation of the numerical approximation error is addressed. An adaptive mesh is utilized to capture the dramatic changes of the option value in a certain critical region. Excellent enhancement of efficiency and accuracy is achieved by the DSC algorithm. With a relatively low computational cost, the final results are accurate to eight significant figures, which is over three orders of magnitude better than the FD scheme based on the same adaptive mesh. For non-dividend paying case, the DSC results achieve the same high accuracy level as those of the higher order of convergence binomial methods.

In the second class of problems, we consider the American option pricing. The first problem in this class is the valuation of American calls on discrete dividend paying assets. By using a reasonable mesh, we obtain results with errors as small as 10^{-8} in all the DSC computations, which is at least four orders of magnitude better than the explicit FD (EFD) scheme based on the same adaptive mesh. The second problem considered includes three kinds of American options. Their exercise boundaries are similar and the closed form analytical pricing formulas do not exist. The benchmark values are calculated by using a standard binomial tree method, with a very high time refinements. Our results are in excellent agreement with the benchmark values. However, the computational cost of the binomial tree method is from 18270 to 35238 times larger than that of the DSC algorithm. For this American option valuation problem, numerical convergence test shows that although the displayed spatial discretization order of the DSC algorithm is only slightly higher than that of the EFD

scheme, the DSC scheme does have much smaller approximation error. Based on the same adaptive mesh, the DSC results are 10 times more accurate than those of the EFD scheme, so that a larger computational effort is required for the EFD scheme to achieve the same level of accuracy as the DSC scheme. Two extended lattice approaches are also employed for the valuation of American puts on non-dividend paying assets. Again, results of the same accuracy level are obtained by both high accuracy binomial models and the DSC scheme. However, the DSC is computationally cheaper than these two binomial models. The last problem considered is the valuation of American puts on discrete dividend paying assets (APDD). The optimal exercise boundaries of APDD are approximated by using the DSC algorithm. The results match well with theoretical ones. These studies indicate that the DSC algorithm is efficient, accurate, and reliable for numerical option valuation problems.

Appendix A. DSC differential kernels

The differentiation in Eq. (29) can be easily carried out for a given $\delta_{\alpha,\beta;k}(x)$. For example, if

$$\delta_{\frac{\pi}{\Delta},\beta;k}(x) = \frac{\sin\frac{\pi}{\Delta}(x-x_k)}{\frac{\pi}{\Delta}(x-x_k)} e^{-((x-x_k)^2/2\beta^2)}, \tag{A.1}$$

we have for $x \neq x_k$ [41]

$$\delta^{(1)}_{\frac{\pi}{\Delta},\beta;k}(x) = \left\{ \frac{\cos\frac{\pi}{\Delta}(x-x_k)}{(x-x_k)} - \frac{\sin\frac{\pi}{\Delta}(x-x_k)}{\frac{\pi}{\Delta}(x-x_k)^2} - \frac{\sin\frac{\pi}{\Delta}(x-x_k)}{\frac{\pi}{\Delta}\beta^2} \right\} \times \exp\left(-\frac{(x-x_k)^2}{2\beta^2} \right), \tag{A.2}$$

and

$$\delta^{(2)}_{\frac{\pi}{\Delta},\beta;k}(x) = \left\{ -\frac{\frac{\pi}{\Delta}\sin\frac{\pi}{\Delta}(x-x_k)}{(x-x_k)} - 2\frac{\cos\frac{\pi}{\Delta}(x-x_k)}{(x-x_k)^2} - 2\frac{\cos\frac{\pi}{\Delta}(x-x_k)}{\beta^2} + 2\frac{\sin\frac{\pi}{\Delta}(x-x_k)}{\frac{\pi}{\Delta}(x-x_k)^3} + \frac{\sin\frac{\pi}{\Delta}(x-x_k)}{\frac{\pi}{\Delta}(x-x_k)\beta^2} + \frac{\sin\frac{\pi}{\Delta}(x-x_k)}{\frac{\pi}{\Delta}\beta^4}(x-x_k) \right\} \times \exp\left(-\frac{(x-x_k)^2}{2\beta^2} \right). \tag{A.3}$$

At $x = x_k$, it is convenient to evaluate these derivatives separately

$$\delta^{(1)}_{\frac{\pi}{\Delta},\beta;k}(x_k) = 0, \text{ and } \delta^{(2)}_{\frac{\pi}{\Delta},\beta;k}(x_k) = -\frac{1}{3}\frac{3+\frac{\pi^2}{\Delta^2}\beta^2}{\beta^2}. \tag{A.4}$$

Similarly, the differentiation in Eq. (29) can also be easily carried out for a finite Lagrange kernel

$$\delta_{\alpha,\beta;k}(x) = \prod_{i=-W,i\neq k}^{W} \frac{x - x_i}{x_k - x_i}. \tag{A.5}$$

We have

$$\delta^{(1)}_{\alpha,\beta;k}(x) = \sum_{j=-W,j\neq k}^{W} \frac{1}{x_k - x_j} \prod_{i=-W,i\neq k,j}^{W} \frac{x - x_i}{x_k - x_i}, \tag{A.6}$$

$$\delta^{(2)}_{\alpha,\beta;k}(x) = \sum_{j,m=-W,j\neq k,m\neq k,m\neq j}^{W} \frac{1}{(x - x_j)(x - x_m)} \prod_{i=-W,i\neq k,j,m}^{W} \frac{x - x_i}{x_k - x_i}. \tag{A.7}$$

Note that the differentiation matrix in Eq. (28) is in general banded. This gives rise to great advantage in large scale computations. Extensions to higher dimensions can be realized by tensorial products.

Appendix B. Analytic pricing formulae

For a European call option, the analytic Black–Scholes fair value can be solved exactly from Eqs. (4), (40), and (41) [5],

$$v(S,\tau) = S\mathrm{e}^{-q\tau}N(d_1) - X\mathrm{e}^{-r\tau}N(d_2), \tag{B.1}$$

where

$$d_1 = \frac{\ln\frac{S}{X} + \left(r - q + \frac{\sigma^2}{2}\right)\tau}{\sigma\sqrt{\tau}}, \quad d_2 = d_1 - \sigma\sqrt{\tau}, \tag{B.2}$$

and $N(\cdot)$ is the cumulative probability distribution function for a standardized normal variable:

$$N(u) = \frac{1}{\sqrt{2\pi}} \int_{-\infty}^{u} \mathrm{e}^{-x^2/2}\,\mathrm{d}x. \tag{B.3}$$

The formula for the value of an American call option on a stock paying a single dividend was suggested by Roll [33], Geske [17] and Whaley [39]

$$\begin{aligned} v(\tilde{S},\tau) = {} & \tilde{S}\left[1 - N_2\left(-a_1, -b_1; \sqrt{\frac{\tau - \tau_d}{\tau}}\right)\right] + D\mathrm{e}^{-r(\tau-\tau_d)}N(a_2) \\ & - X\left[\mathrm{e}^{-r(\tau-\tau_d)}N(a_2) + \mathrm{e}^{-r\tau}N_2\left(-a_2, b_2; -\sqrt{\frac{\tau - \tau_d}{\tau}}\right)\right], \end{aligned} \tag{B.4}$$

where

$$a_1 = \frac{\ln\frac{\tilde{S}}{\tilde{S}^*} + (r + \frac{\sigma^2}{2})(\tau - \tau_d)}{\sigma\sqrt{\tau - \tau_d}}, \quad a_2 = a_1 - \sigma\sqrt{\tau - \tau_d},$$
$$b_1 = \frac{\ln\frac{\tilde{S}}{X} + (r + \frac{\sigma^2}{2})\tau}{\sigma\sqrt{\tau}}, \quad b_2 = b_1 - \sigma\sqrt{\tau}. \tag{B.5}$$

Here $N_2(a,b;\rho)$ is the standard bivariate normal distribution function with correlation coefficients ρ

$$N_2(a,b;\rho) = \int_{-\infty}^{a}\int_{-\infty}^{b} \frac{1}{2\pi}\frac{1}{\sqrt{1-\rho^2}} \times \exp\left(-\frac{x'^2 - 2\rho x'y' + y'^2}{2(1-\rho^2)}\right) dx'\,dy', \tag{B.6}$$

and $\tilde{S}^*$ is given by the solution of algebraic equation

$$\tilde{S}^* + D - X = v(\tilde{S}^*, \tau_d), \tag{B.7}$$

where $v(\tilde{S}^*, \tau d)$ is the European call price given by the Black–Scholes formula. It can be shown mathematically that $D > X[1 - e^{-r\tau_d}]$ is a necessary condition for the existence of solution to Eq. (B.7). The generalization of the above price formula to multiple discrete dividends was discussed by Selby and Hodges [35].

References

[1] K. Amin, A. Khanna, Convergence of American option values from discrete- to continuous-time financial models, Math. Financ. 4 (1994) 289–304.
[2] G. Bao, G.W. Wei, S. Zhao, Local spectral time-domain method for electromagnetic wave propagation, Opt. Lett. 28 (2003) 513–515.
[3] G. Bao, G.W. Wei, S. Zhao, Numerical solution of the Helmholtz equation with high wavenumbers, Int. J. Numer. Meth. Engng. 59 (2004) 389–408.
[4] G. Barone-Adesi, R.E. Whaley, Efficient analytic approximation of American option values, J. Financ. 42 (1987) 301–320.
[5] F. Black, M. Scholes, The pricing of options and corporate liabilities, J. Polit. Econ. 81 (1973) 637–659.
[6] P. Boyle, Options: a Monte Carlo approach, J. Financ. Econ. 44 (1977) 323–338.
[7] M. Brennan, E. Schwartz, The valuation of American put options, J. Financ. 32 (1977) 449–462.
[8] M. Brennan, E. Schwartz, Finite difference methods and jump processes arising in the pricing of contingent claims: a synthesis, J. Financ. Quant. Anal. 13 (1978) 461–474.
[9] M. Broadie, J. Detemple, American option valuation: new bounds, approximations, and a comparison of existing methods, Rev. Financ. Stud. 9 (1996) 1211–1250.
[10] G.W. Buetow, J.S. Sochacki, The trade-off between alternative finite difference techniques used to price derivative securities, Appl. Math. Comput. 115 (2000) 177–190.
[11] D.S. Bunch, H.E. Johnson, A simple and numerically efficient valuation method for American puts using a modified Geske-Johnson approach, J. Financ. 47 (1992) 809–816.

[12] P. Carr, D. Faguet, Fast accurate valuation of American options, Working paper of Cornell University, 1994.
[13] N. Clarke, K. Parrott, Multigrid for American option pricing with stochastic volatility, Appl. Math. Financ. 6 (1999) 177–195.
[14] G. Courtadon, A more accurate Finite Difference approximation for the valuation of options, J. Financ. Quant. Anal. 17 (1982) 697–703.
[15] J.C. Cox, S.A. Ross, M. Rubinstein, Option pricing: a simplified approach, J. Financ. Econ. 7 (1979) 229–263.
[16] S. Figlewski, B. Gao, The adaptive mesh model: a new approach to efficient option pricing, J. Financ. Econ. 53 (1999) 313–351.
[17] R. Geske, A note on an analytical valuation formula for unprotected American call options on stocks with known dividends, J. Financ. Econ. 7 (1979) 375–380.
[18] R. Geske, H.E. Johnson, The American put option valued analytically, J. Financ. 39 (1984) 1511–1524.
[19] R. Geske, K. Shastri, Valuation by approximation: a comparison of alternative option valuation techniques, J. Financ. Quant. Anal. 20 (1985) 45–71.
[20] J. Hull, A. White, The use of the control variate technique in option pricing, J. Financ. Quant. Anal. 23 (1988) 237–251.
[21] J. Hull, A. White, Valuing derivative securities using the explicit finite different method, J. Financ. Quant. Anal. 25 (1990) 87–100.
[22] P. Jaillet, D. Lamberton, B. Lapeyre, Variational inequalities and the pricing of American options, Acta Appl. Math. 21 (1990) 263–289.
[23] R. Jarrow, A. Rudd, Option Pricing, Irwin, Homewood, 1983.
[24] H.E. Johnson, An analytic approximation for the American put price, J. Financ. Quant. Anal. 18 (1983) 141–148.
[25] Y. Kwok, Mathematical Models of Financial Derivatives, Springer-Verlag, Singapore, 1998.
[26] D.P.J. Leisen, Pricing the American put option: A detailed convergence analysis for binomial models, J. Econ. Dyn. Control 22 (1998) 1419–1444.
[27] D.P.J. Leisen, The random-time binomial model, J. Econ. Dyn. Control 23 (1999) 1355–1386.
[28] D.P.J. Leisen, M. Reimer, Binomial models for option valuation – examining and improving convergence, Appl. Math. Financ. 3 (1996) 319–346.
[29] J. Lund, K.L. Bowers, Sinc Methods for Quadrature and Differential Equations, SIAM, 1992.
[30] L.W. MacMillan, Analytic approximation for the American put option, Adv. Futures Options Res. 1 (1986) 119–139.
[31] R.C. Merton, Theory of rational option pricing, Bell J. Econ. 4 (1973) 141–183.
[32] L.W. Qian, On the regularized Whittaker–Kotel'nikov–Shannon sampling formula, Proc. Amer. Math. Soc. 131 (2003) 1169–1176.
[33] R. Roll, An analytic valuation formula for unprotected American call options on stocks with known dividends, J. Financ. Econ. 5 (1977) 251–258.
[34] E. Schwartz, The valuation of warrants: Implementing a new approach, J. Financ. Econ. 4 (1977) 79–93.
[35] M.J.P. Selby, S.D. Hodges, On the evaluation of compound options, Manage. Sci. 33 (1987) 347–355.
[36] C.E. Shannon, A mathematical theory of communication, AT&T Tech. J. 27 (1948) 379–423.
[37] Z.H. Shao, G.W. Wei, S. Zhao, DSC time-domain solution of Maxwell's equations, J. Comput. Phys. 189 (2003) 427–453.
[38] Y. Tian, A modified lattice approach to option pricing, J. Futures Markets 13 (1993) 563–577.
[39] R. Whaley, On the valuation of American call options on stocks with known dividends, J. Financ. Econ. 9 (1981) 207–211.
[40] D.C. Wan, B.S.V. Patnaik, G.W. Wei, Discrete singular convolution-finite subdomain method for the solution of incompressible viscous flows, J. Comput. Phys. 180 (2002) 229–255.

[41] G.W. Wei, Quasi-wavelets and quasi interpolating wavelets, Chem. Phys. Lett. 296 (1998) 215–222.
[42] G.W. Wei, Discrete singular convolution for the solution of the Fokker–Planck equation, J. Chem. Phys. 110 (1999) 8930–8942.
[43] G.W. Wei, A unified approach for the solution of the Fokker-Planck equation, J. Phys. A: Math. Gen. 33 (2000) 4935–4953.
[44] G.W. Wei, Wavelets generated by using discrete singular convolution kernels, J. Phys. A: Math. Gen. 33 (2000) 8577–8596.
[45] G.W. Wei, Y. Gu, Conjugated filter approach for solving Burger's equation, J. Comput. Appl. Math. 149 (2002) 439–456.
[46] G.W. Wei, Y.B. Zhao, Y. Xiang, Discrete singular convolution and its application to the analysis of plates with internal supports I. Theory and algorithm, Int. J. Numer. Meth. Engng. 55 (2002) 913–946.
[47] Y. Xiang, Y.B. Zhao, G.W. Wei, Discrete singular convolution and its application to the analysis of plates with internal supports. II Complex supports, Int. J. Numer. Meth. Engng. 55 (2002) 947–971.
[48] S. Zhao, G.W. Wei, Comparison of the discrete singular convolution and three other numerical schemes for solving Fisher's equation, SIAM J. Sci. Comput. 25 (2003) 127–147.